2026 IEEE International Conference on Robotics and Automation (ICRA 2026)
June 1-5, 2026. Vienna, Austria

Evolutionary Automatic Guidance Scheme for Magnetic Nanoparticles in High-Flow Vascular Models Using a Uniform Magnetic Force Field

Boyoung Son, Metin Sitti and Jungwon Yoon

Abstract— **Magnetic nanoparticle (MNP) guidance has attracted considerable attention for biomedical applications, such as targeted drug delivery and minimally invasive therapy. However, precise navigation in vivo remains challenging, particularly in high-flow vascular environments, where drag forces dominate particle dynamics and real-time feedback is impractical. Here, we present an evolutionary automatic guidance scheme for feedforward control of MNP chains in a vascular model. The proposed approach leverages chain alignment with the flow direction to achieve directional migration into specific branches, without relying on swarm cohesion or online feedback. To provide uniform actuation, a Halbach array is designed and optimized to generate a nearly uniform magnetic force field within the target workspace. A physics-based simulator incorporating magnetic, drag, and wall interaction forces is developed to model chain dynamics, and control sequences are optimized using the Covariance Matrix Adaptation Evolution Strategy (CMA-ES), ensuring robustness to variations in chain length and injection conditions. The method is experimentally validated using a four-channel vascular model, demonstrating that feedforward magnetic actuation can reliably guide nanoparticle chains under physiologically relevant high-flow conditions. This study establishes a practical and scalable strategy for nanoparticle navigation, providing a foundation for future biomedical applications in dynamic vascular environments.**

I. Introduction

Nanorobotics has emerged as a transformative technology for next-generation medical applications, including targeted drug delivery, biosensing, and minimally invasive therapies [1]. Among various actuation modalities—such as electric fields, ultrasound, and light—magnetic actuation has proven particularly effective [2, 3]. Magnetic fields penetrate deep into biological tissue with minimal attenuation, are non-ionizing and biocompatible, and are scalable to the nanoscale, making them ideally suited for biomedical manipulation [4, 5].

Magnetic nanoparticles (MNPs) provide unique advantages in this context. Due to their small size, MNPs can cross biological barriers inaccessible to microrobots, such as the blood–brain barrier (BBB) [6]. For instance, arterial injection of nanoparticles has been proposed to deliver therapeutic agents directly into cerebral vessels [7]. However, guiding MNPs through fast-flowing arterial environments remains challenging. Arterial blood flow, with velocities of several centimeters per second, generates strong drag forces that dominate nanoparticle dynamics. Under these conditions, conventional swarm-based approaches may lose cohesion, making reliable navigation difficult.

Various strategies have been explored for magnetic nanoparticle guidance, including MRI-based gradient steering [8], swarm-based control relying on dipole–dipole interactions [9], and closed-loop strategies using real-time imaging feedback [10]. While effective in certain contexts, these approaches face limitations in high-flow environments. MRI-based methods are constrained by gradient pulse sequences, restricting trajectory complexity; swarm-based control can fail under strong arterial shear; and closed-loop imaging is limited by finite temporal resolution. These challenges highlight the need for feedforward strategies capable of guiding nanoparticles reliably without relying on swarm cohesion or real-time feedback.

To address these challenges, we propose an evolutionary automatic guidance scheme for MNP chains in high-flow vascular models. Unlike conventional swarm-based control, our approach focuses on guiding chain-like bundles naturally formed by dipole–dipole interactions. A critical limitation of standard Helmholtz coil-based methods is the rapid loss of control authority as magnetic field gradients become non-uniform, especially when flow-induced dispersion increases inter-chain spacing.

Our system overcomes this limitation by generating a nearly uniform magnetic force field and controlling the orientation of chains collectively. Even when inter-chain spacing varies, particles within the same branch are guided along consistent trajectories.

This proposed framework is implemented in three stages: (i) the design of a hybrid dipole–quadrupole Halbach array for uniform force generation, (ii) the development of a Vascular Magnetic Particle Chain (VMC) simulator that models chain dynamics under complex forces, and (iii) the optimization of feedforward control commands.

Experimental results demonstrate that the evolutionary automatic guidance scheme achieves robust and reproducible steering of magnetic nanoparticle chains in high-flow vascular environments. Compared to uncontrolled injections, the proposed framework more than doubles the success rate of guiding chains into the target branch, confirming that reliable navigation is achievable even when inter-chain spacing varies due to flow-induced dispersion. These findings establish a foundation for precise nanoparticle delivery under physiologically relevant flow conditions, supporting applications in targeted therapy, brain therapeutics, and minimally invasive interventions.

Boyoung Son is with the School of Integrated Technology, Gwangju institute of Science and Technology, Gwangju 61005, Korea e-mail: sonboyoung@gm.gist.ac.kr).

Metin Sitti is with the Max Planck Institute of Physical Intelligent systems, Stuttgart, 70569, Germany and School of Medicine and College of Engineering, Koç University, Istanbul 34450, Turkey (e-mail: Sitti@is.mpg.de).

Jungwon Yoon is with the School of Integrated Technology, Gwangju institute of Science and Technology, Gwangju 61005, Korea (corresponding author to provide phone: +82 10- 2402-6904; e-mail: jyoon@gist.ac.kr).

II. METHOD

The primary objective of this study is to design a control system for magnetic nanoparticle chains under high-flow conditions. To ensure feasibility before constructing the experimental setup, the target operating conditions were defined. We assumed a tubular channel with a radius of 1 mm and a maximum flow velocity of 50mm/s along the centerline. The nanoparticles were modeled as superparamagnetic spherical Fe_3O_4 particles, average diameter of 20nm ($\sigma \approx$ 5nm), density $\rho \approx 5.17$ g/cm³, and saturation magnetization $M_s \approx 70$ emu/g

In the proposed guidance scheme, we focus on controlling individual magnetic nanoparticle chains rather than swarm formations. In realistic vascular environments, MNPs tend to aggregate into chain bundles along vessel walls due to dipole–dipole interactions. These chains exhibit strong internal cohesion, and their deformation under typical actuation forces is negligible. Therefore, in our model, inter-chain interactions are ignored, and simulations are performed for a single representative chain. The guidance framework is designed to steer these randomly distributed chains such that they align along the desired branch, despite variations in initial positions or chain lengths. To achieve this, a uniform magnetic force field is generated, ensuring that each chain experiences nearly identical forces regardless of its spatial location. By maintaining consistent chain orientation along the target trajectory, this method achieves robust navigation in high-flow conditions, regardless of increased inter-chain spacing.

A. Forces Acting on Magnetic Nanoparticle Chain

The forces acting on magnetic nanoparticle chains in a fluid environment can be described by combining magnetic, drag, and wall interaction contributions. Although individual nanoparticles experience additional forces such as interparticle dipole and repulsive interactions, gravity, and chain-to-chain interactions, these internal forces are relatively small under high-flow conditions. As a result, each chain can be modeled as a single rigid body, allowing the simulation to focus on the dominant contributions: magnetic force F_{mag}, fluid drag F_{drag}, and wall interactions F_{wall} (1)

$$\mathrm{F} = F_{mag} + F_{drag} + F_{wall} \tag{1}$$

The magnetic force is expressed as follows:

$$F_{mag} = \sum_{n} \mu_0 V (M(H) \cdot \nabla) H \tag{2}$$

where μ_0 is the permeability of free space, n is the number of particles forming the particle chain, V is the particles volume, M(H) is the magnetization of the particles, and ∇H denotes the gradient of the applied magnetic field.

The drag force is expressed as follows:

$$F_{drag} = \sum_{n} -6\pi\eta R v_{rel} \tag{3}$$

where η is the viscosity, R is the radius of particles, and v_{rel} is the relative velocity of the chain with respect to the fluid. Although hydrodynamic interactions are complex due to the nonlinear nature of the Navier-Stokes equations [11], they are neglected here to reduce the computational burden. In this simulation, the Reynolds number is calculated at a value much smaller than 1. Therefore, we ignore higher-order terms and use a simplified model.

From these expressions, it is evident that the forces acting on the chain strongly depend on its position within the flow. Under high-flow conditions, drag dominates over dipole–dipole interactions, causing chains to move individually rather than as a cohesive swarm. We aim to develop a control system robust to inter-chain dispersion, ensuring consistent guidance even when chains spread apart. Conventional two-magnet configurations, such as FFP-based approaches, exhibit large position-dependent force variations and are sensitive to disturbances [12]. To overcome these limitations, a dipole–quadrupole Halbach-inspired magnetic field is adopted [13], providing a more uniform force distribution and forming the foundation of the proposed guidance system.

B. Uniform Magnetic Force Field Using a Halbach Array

As discussed above, a key requirement for reliable guidance is that nanoparticle chains experience nearly identical magnetic forces throughout the target region. This uniformity can be achieved using a hybrid dipole–quadrupole Halbach array [14].

To address these challenges, we designed an optimized Halbach array tailored to the experimental setup. The array consists of 24 *NdFeB* magnets (*N35* grade, 20×20×40mm), arranged to generate a uniform gradient field within a cylindrical region 70mm in diameter. Assuming magnetic saturation, *M(H)* can be treated as constant, which reduces the magnetic force expression (2) to a form directly proportional to the field gradient ∇H. Consequently, the optimization objective was defined as achieving a uniform field gradient within the target workspace.

As illustrated in Fig. 1, the baseline geometry comprises two dipole arrays placed symmetrically around a central quadrupole array. Each array contains 8 magnets, and the overall radius is fixed at 110mm to ensure manufacturability. The dipole arrays establish the baseline field intensity $|H|$, while the quadrupole array shapes the spatial gradient. Modifying the dipole arrays could reduce the overall field strength, complicating the objective function for optimization; therefore, in this study, the dipole arrays are kept fixed while only the quadrupole array is optimized.

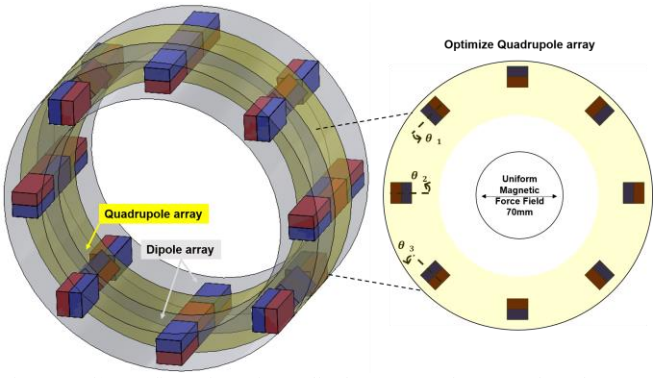

Fig. 1 (Left) Configuration of two dipole arrays and one quadrupole array. (Right) Optimization criteria and parameter settings for the optimized quadrupole array.

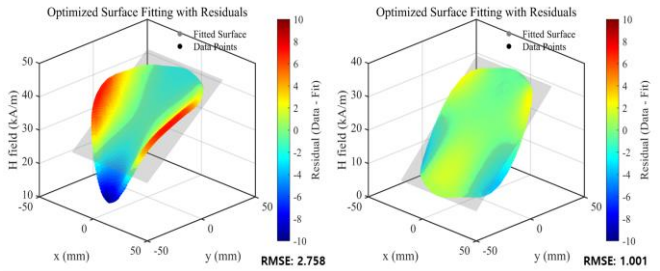

Fig. 2 Visualization of magnetic field *H* data when fitted to a plane. The left side shows an RMSE value of 2.758, and the right side shows an RMSE value of 1.001. It can be seen that the smaller the error in the magnetic field plane fitting, the more uniform the magnetic field gradient is generated.

By superimposing these configurations, the composite array achieves sufficient field strength and a uniform gradient, enabling precise control of the magnetic force distribution. The variations in the quadrupole magnet orientation significantly affect the resulting magnetic field distribution. Due to the intrinsic symmetry of the quadrupole array, the entire arrangement can be fully determined by specifying only three independent magnet angles.

The primary objective of the optimization was to generate a spatial region with a uniform magnetic force, enabling consistent control of particles. In this study, the magnetic field was initially configured such that the gradient$\nabla H$is predominantly aligned along a single direction and exhibits smooth spatial variation. Under these conditions, the scalar field magnitude $|H|$ serves as a reliable proxy for assessing gradient uniformity. To quantify uniformity, the spatial distribution of $|H|$ was approximated by a planar function:

$$H(x,y) \approx ax + by + c \tag{4}$$

If the magnetic field gradient is truly uniform, the measured field should closely follow this planar profile. Consequently, the deviation between the actual field and the fitted plane provides a direct measure of non-uniformity. This deviation between the simulated field values $\hat{H}_i$ and the fitted plane values H_i was quantified by the RMSE:

$$RMSE = \sqrt{\frac{1}{N}\sum_{i=1}^{N}\left(\hat{H}_i - H_i\right)^2} \tag{5}$$

Minimizing this RMSE promotes a more uniform scalar field, corresponding to a consistent ∇H across the region of interest. Because the initial field gradient is largely aligned, using $|H|$ planar fitting as the optimization metric introduces negligible error relative to directly evaluating ∇H. Based on this definition, the optimization problem was formulated as determining the magnet orientation parameters $(\theta_1, \theta_2, \theta_3)$ that minimize the RMSE (6)

$$\theta_1^*, \theta_2^*, \theta_3^* = arg \min_{\theta_1,\theta_2,\theta_3} RMSE(\theta_1, \theta_2, \theta_3) \tag{6}$$

Consequently, this approach provides an experimentally accessible and physically meaningful objective function for optimizing the magnet array. Fig. 3 shows the results of the optimization, which was carried out using a gradient descent algorithm. The rotation angle of the magnets is set as a constraint to avoid creating duplicate arrays.

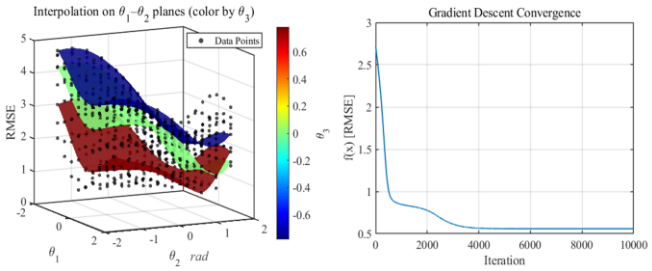

Fig. 3 (Left) Graph interpolating simulated data. (Right) Gradient Descent convergence graph. The minimum value was determined from the interpolated data.

TABLE I. HALBACH ARRAY OPTIMIZATION CONDITION

Description	Value
Learning rate	1×10^{-3}
Initial value	$(\theta_1, \theta_2, \theta_3) = (0, 0, 0)$
Boundary condition	$\theta_{1,2,3} = [-\frac{\pi}{2}, \frac{\pi}{2}]$
Convergence conditions	$\varepsilon < 1 \times 10^{-8}$
Finite difference step size	$\delta = 1 \times 10^{-5}$

TABLE II. HALBACH ARRAY OPTIMIZATION RESULTS

θ_1	θ_2	θ_3	RMSE	$\lvert\nabla H(x,y)\rvert$
-29.44°	78.57°	22.53°	0.4579	5.14×10^5 [A/m^2]

A spline interpolation was employed to represent the angular parameters of the quadrupole array, which were iteratively updated to minimize the RMSE. The conditions used in the optimization algorithm are as shown in Table 1, and the final optimized angle values of the array elements are summarized in Table 2. This approach allowed for systematic refinement of the quadrupole configuration, yielding a more uniform field gradient while preserving the baseline field magnitude established by the dipole array. As a result, the optimized Halbach array provides an almost uniform gradient field across the 70mm region, thereby ensuring spatially consistent magnetic forces for nanoparticle chain manipulation and enhancing the robustness of field-driven actuation.

The entire array can be rotated to change the force direction, forming the core actuation mechanism of our uniform magnetic force system. While the individual magnet array could in principle be rotated separately, our objective is to generate a globally uniform magnetic force field to control nanoparticle chains. Therefore, the positions of the magnets are fixed relative to each other, and the array is rotated as a whole, allowing the system to adjust only the direction of the magnetic force while maintaining its magnitude, thereby ensuring effective and reproducible particle guidance.

C. Vascular Magnetic Particle Chain Simulator Design

To implement the proposed guidance scheme, we developed a Vascular Magnetic Particle Chain (VMC) simulator that replicates the experimental high-flow environment. Focusing on the dynamics of individual chains, each nanoparticle chain is modeled as a rigid rod rather than as discrete nanoparticles, and deformation effects are neglected in the current analysis.

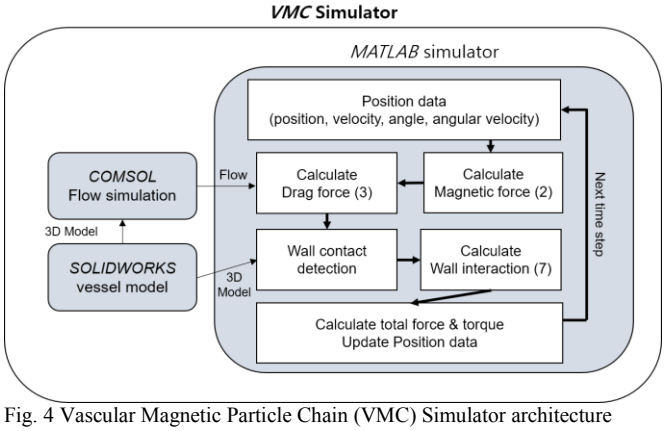

Fig. 4 Vascular Magnetic Particle Chain (VMC) Simulator architecture

To reflect the experimental scenario, a vascular-inspired model with four outlet branches was constructed. The model fits within the 70mm target region and assumes an input water flow velocity of 50mm/s. While nanoparticle guidance in two-channel vessels can be readily achieved using simple methods, the present study investigates whether similar guidance can be extended to a more complex four-branch configuration. In particular, the guidance performance in inner branch, representing the most challenging path, was evaluated as a critical indicator of the system's effectiveness.

The simulator was implemented by first performing flow field simulations in COMSOL and then importing the results into MATLAB for chain dynamics modeling in Fig. 4. The governing forces are summarized in (1). The magnetic force is given by (2), where ∇H is already computed from the optimized Halbach design. The drag force is given by (3), based on the simulated flow field. In reality, complex interactions between particles and walls are at play [15].

However, for simplicity, we simulate only the simplest form of the interaction. Wall interactions are modeled as in (7), consisting of normal and frictional components.

$$F_{wall} = F_{normal} + F_{friction}$$

$$\vec{F}_{friction} = \begin{cases} -\vec{F}_{\parallel}, \ if \ |\vec{F}_{\parallel}| \le \mu_s |\vec{F}_{normal}| \\ -\mu_k \vec{F}_{normal} \dfrac{\vec{F}_{\parallel}}{|\vec{F}_{\parallel}|}, \ if \ |\vec{F}_{\parallel}| > \mu_s |\vec{F}_{normal}| \end{cases} \quad (7)$$

$F_{\parallel}$ is the component of the force parallel to the wall, μ_s is the coefficient of static friction and μ_k is the coefficient of kinetic friction. Frictional effects were experimentally estimated by observing chain motion in a real tube under equivalent flow conditions. Since chains are treated as rigid bodies, torque effects must also be considered, as summarized in (8).

$$\vec{\tau}_{mag} = \int \mu_0 V M_{sat} (\hat{m} \times \vec{H})$$

$$\vec{\tau}_{drag} = \sum_{i=1}^{n} (\vec{x}_i - \vec{x}_0) \times \vec{F}_{drag}^{(i)}$$

$$\vec{\tau}_{normal} = (\vec{x}_n - \vec{x}_0) \times \vec{F}_{normal}$$

$$\vec{\tau}_{friction} = (\vec{x}_n - \vec{x}_0) \times \vec{F}_{friction} \quad (8)$$

$\hat{m}$ is the unit vector of the magnetization direction, M_{sat} is the *M(H)* value when the particle is saturated, *V* is the volume of the MNP, and $\vec{H}$ is the magnetic field. The magnetization direction in the chain is assumed to be the angle of the chain, and all particles within the chain are assumed to have the same magnetization direction. *n* is the number of times the chain is divided, we find an appropriate value that does not excessively increase the amount of flow calculations and causes less error. $\vec{x}$ is the displacement of each part of the chain. The chain length was determined according to (9), following the equilibrium analysis described in MJ. Park′s work [16].

$$L = R - d + R\sqrt[\varsigma]{1 - \frac{\max\left(\frac{dU_m}{dD}\right)}{3\pi\eta d v_{\perp}}}$$

$$v_{\perp} = V_{max}\left(1 - \left(\frac{r}{R}\right)^{\varsigma}\right) \quad (9)$$

U_m is average magnetic dipolar energy between a magnetic chain and magnetic particle. $v_{\perp}$ is the flow velocity in the radial direction, V_{max} is the centerline maximum flow velocity. r is the axial location of particle, and *R* is the radius of the channel. ς is a constant for a particular profile. *D* is breaking displacement, η is viscosity, and *d* is the radius of particle. The length of the chain is determined by the point where the drag force and dipole force are in equilibrium. Simulation parameters are listed in Table 3.

D. Guidance Command Generation

Guidance commands can be generated using various strategies, including haptic-device-based manual input, reinforcement learning, and optimization-based approaches [17-19]. In this work, an evolutionary automatic guidance scheme is employed to compute feedforward control sequences for nanoparticle chains. As illustrated in Fig. 5, nanoparticle chains are injected at *z* = +5mm with the initial magnetic field aligned along the +*X* axis. The control input corresponds to the rotation angle of the magnet array, which determines the direction of the magnetic force.

TABLE III. VMC SIMULATOR PARAMETERS

Description	Parameters	Value
Radius(particle)	d	20 [nm]
Density(particle)	ρ	5.17×10^3 [kg/m^3]
Viscosity(water)	η	0.001 [Pa· s]
Magnetization(saturated)	M_{sat}	3.57×10^5 [A/m]
Coefficient (kinetic friction)	μ_k	0.4
Coefficient (static friction)	μ_s	0.5
Gradient H	$\|\nabla H\|$	5.14×10^5[A/m^2]
Time step	Δt	2×10^{-5}[s]
Simulation time	t	8 [s]
Chain Length	L	1.61 [mm]
Chain divided time	n	50

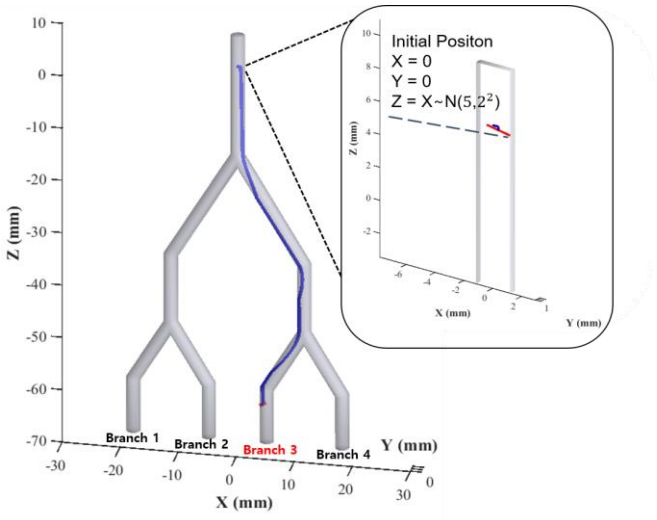

Fig. 5 Simulation visualization 3D. Chain movement path (blue line) and Chain position (red). The initial injection position is determined randomly only by the z value. Since the initial magnet system angle is set to the $+X$ direction, the MNP chain naturally attaches to the wall and begins guidance in that state.

The objective is to direct chains into branch3. The command sequence is parameterized as a sinusoidal trajectory of rotation angles (10)

$$\theta_{controll}(t) = A_1 \sin(w_1 t + \varphi_1) + A_2 \sin(w_2 t + \varphi_2) \quad (10)$$

To capture the inherent variability in chain configurations upon injection, the initial positions and lengths of nanoparticle chains are randomized. Even when the injection point is fixed, chains naturally disperse around the injection site and adhere to the vessel walls, resulting in slight variations in both chain position and length. To reflect this, the initial chain lengths and positions are modeled as normally distributed variables.

Since chains attach to the vessel walls, their initial positions are randomized only along the Z-axis, parallel to the walls. The guidance command is then activated once the chains naturally adhere to the wall at x=1mm, under the initial uniform magnetic force oriented along the $+X$ direction. To account for variability in chain length and injection position, 100 randomized simulations are conducted per iteration, and the proportion of chains reaching branch 3 is evaluated. Since the outer branch is relatively easy to induce, we targeted branch 3 to verify the effectiveness of guidance. This setup reflects the practical need to guide multiple chains simultaneously, ensuring that all chains adopt the command with the highest probability of reaching the target.

The Covariance Matrix Adaptation Evolution Strategy (CMA-ES), a derivative-free algorithm suitable for optimizing non-differentiable or noisy objectives, is used to update the parameter distribution and maximize success probability, as illustrated in Fig. 6. By iteratively adjusting the distribution based on observed outcomes, CMA-ES converges to a fixed command sequence that robustly guides particles into the target branch, effectively handling uncertainties in injection and chain length. The optimization conditions are listed in Table 4. Boundary conditions are set by constraints on the rotational angular velocity of a realistic magnet system and fixed initial positions.

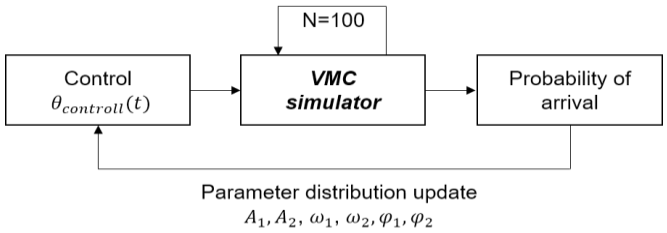

Fig.6 Algorithm structure diagram. N is the number of simulation repetitions

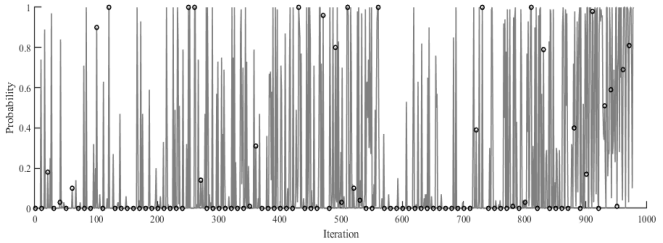

Fig. 7 CMA-ES optimization. Probability over Iterations. Every 10th value is indicated by a dot.

TABLE IV. CMA-ES OPTIMIZATION CONDITIONS

Description	Parameters	Value
Initial position	$Pos[0]$	(0, 0, X~N(μ, σ^2)) $\mu = 5$, $\sigma = 2$ [mm]
Chain Length	L	X~N(μ, σ^2) $\mu = 1.61$, $\sigma = 0.15$ [mm]
Simulation time	Time	8 [s]
Boundary condition		A = [-5, 5] w = [0, 5] $\theta(0) = 0$ $\lvert A_1 + w_1 \rvert + \lvert A_2 + w_2 \rvert < 10$
Goal position (Branch 3)	goal	[5, 1, -67] [mm]

As shown in Fig. 7, the algorithm converged to multiple candidate command sequences achieving near-unity success probabilities (≥0.99), reflecting the presence of multiple equivalent solutions in the probabilistic search space due to the simplicity of the current model. Although chain lengths and initial positions vary, causing individual chains to occupy different positions, the uniform magnetic force field allows consistent control of chain orientation. The angle between the wall and each chain is the dominant factor determining the direction of the forces acting on the chains. In the current simple model, where the wall within a branch is flat, this factor acts similarly across all chains, enabling more consistent and robust guidance despite variations in chain spacing. Importantly, while multiple solutions appear in this simple scenario, the CMA-ES algorithm is capable of identifying globally optimal guidance sequences even in more complex and realistic vascular models.

From these candidate solutions, one sequence was selected based on the criterion of minimizing peak angular acceleration, ensuring stable operation by reducing abrupt torque variations and promoting smooth magnet rotation (11).

$$Control\ \ Command^* = \arg\min_{solution}(\max(\ddot{\theta}_{controll}(t))) \quad (11)$$

TABLE V. CONTROL COMMAND OPTIMIZATION RESULTS

A_1	A_2	ω_1	ω_2	φ_1	φ_2	Probability
-3.32	1.05	1.64	0.17	-0.25	-0.92	1

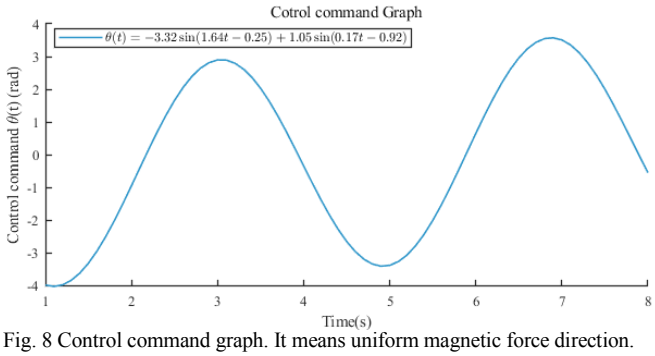

Fig. 8 Control command graph. It means uniform magnetic force direction.

This selection criterion not only favors operational stability but also provides a reproducible and experimentally feasible guidance command. The final command sequence is summarized in Table 5, with its mathematical representation provided in Fig. 8.

III. EXPERIMENT AND RESULT

A. Construction of the Experimental Setup

Based on the previously optimized Halbach array design, a physical magnetic system was constructed. The system consisted of two dipole arrays and one optimized quadrupole array, arranged concentrically in a cylindrical configuration and allowing central-axis rotation. A total of 24 *NdFeB* magnets were embedded within 3D-printed structural components to realize the simulated design. Three arrays (Dipole–Optimized Quadrupole–Dipole) were stacked and assembled to enable rotational actuation, thereby generating a uniform magnetic force in the target region along the desired direction. This configuration reproduced the magnetic field gradient and magnitude predicted by simulations within the 70mm target region, providing a controlled environment for subsequent particle guidance experiments.

The system was coupled with gears and a stepper motor to enable controlled rotation. To verify its performance, a preliminary in-vitro experiment was conducted to evaluate whether magnetic nanoparticles experienced uniform forces within the central 70mm region. Droplets containing Fe_3O_4 nanoparticles (200mg/mL in oil) were prepared, and 0.5μl droplets were deposited at 10mm intervals across the region. Each position was tested five times to account for variability, and the average nanoparticle displacement was measured and plotted.

As shown in Fig. 9, the results exhibited high reproducibility, with trajectories from different initial positions showing near-complete overlap. This indicates that MNPs experienced nearly identical forces throughout the measurement region, providing direct empirical evidence of the spatial uniformity of the generated magnetic field gradient. Moreover, the observed particle displacements closely matched the simulated predictions, confirming that the optimized Halbach array successfully produced a uniform field within the 70mm target area.

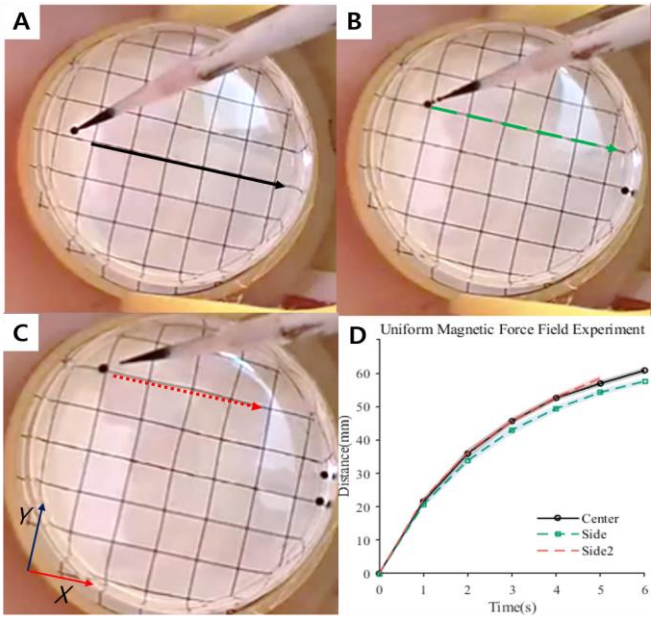

Fig. 9 Uniform magnetic force field test. Nanoparticle droplets The grid spacing is 10mm. The experiment was conducted in three locations: (A) center, (B) side *Y*=10mm, (C) side 2 *Y*=20mm. (D) Average distance graph of magnetic particle droplets at each location. Shading is standard deviation.

B. 4-Channel Model Experiment

To validate the simulation results, an in-vitro experiment was conducted using a four-channel vascular network designed to replicate the modeled flow environment. The network was fabricated with silicone tubes of 1mm radius forming Y-shaped junctions, representing simplified branching vasculature. A syringe pump maintained a steady flow velocity of 50mm/s, and water was used as the working fluid to match the viscosity and flow conditions assumed in the simulation. Fe_3O_4 nanoparticles (10mg, 20nm diameter) were injected at *Z*=+5mm, the same initial injection position used in the simulation. After injection, the particle chains were allowed to settle and adhere to the channel walls, resulting in a distribution along the walls originating from the injection site and establishing consistent initial conditions for the guidance experiment.

The experimental setup, illustrated in Fig. 10, includes the magnetic actuation system, the optimized Halbach array, and the placement of the four-channel network within the workspace. The Halbach array, positioned between two dipole arrays, consists of three magnet rings that rotate together. By the rotation, the direction of the magnetic force within the workspace can be precisely controlled. Prior to particle injection, the magnetic field is aligned along the +*X* axis so that guidance starts with the particle attached to the wall.

Control commands generated by the CMA-ES algorithm (Fig. 8) were applied via an Arduino-controlled stepper motor, rotating the magnet rings together according to the optimized time-dependent trajectory. Particle collection was quantified using a magnetic particle analyzer (*Magquan, MagQu*). This setup ensured faithful reproduction of the simulation-based guidance strategy and allowed quantitative evaluation of particle targeting efficiency. The following procedure was followed to ensure reproducibility and statistical reliability:

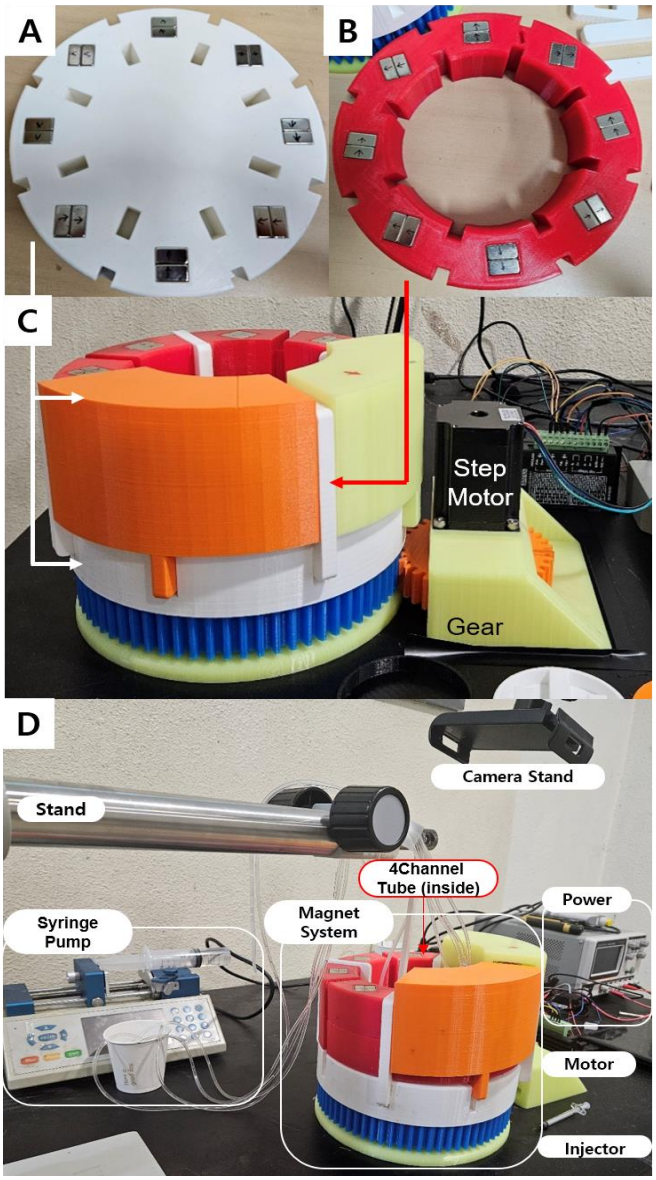

Fig. 10 (A) Dipole array configuration. (B) Optimized array configuration. (C) The final combined magnet system. The Optimized array is located between the two Dipole arrays. (D) 4-Channel Experimental environment configuration. The 4-channels are located inside the magnet system.

1. Prepare a 100mg/ml aqueous suspension Fe_3O_4 magnetic nanoparticles (diameter: 20nm).
2. Inject $0.1ml$ of the suspension (corresponding to 10 mg of particles) at z = 5mm using a syringe.
3. Apply a water flow at 50mm/s using the syringe pump.
4. Activate the control commands to initiate guidance.
5. Collect the particles that arriving at Branch 3 and quantify the collected particles using a magnetic particle measuring instrument (*Magquan, MagQu*).
6. Calculate the transfer ratio by comparing the measured signal of guided particles with the initially injected 10 mg.
7. Repeat the procedure 5 times, discard the highest and lowest values, and calculate the mean of the remaining.
8. Repeat the same procedure without control for comparison.

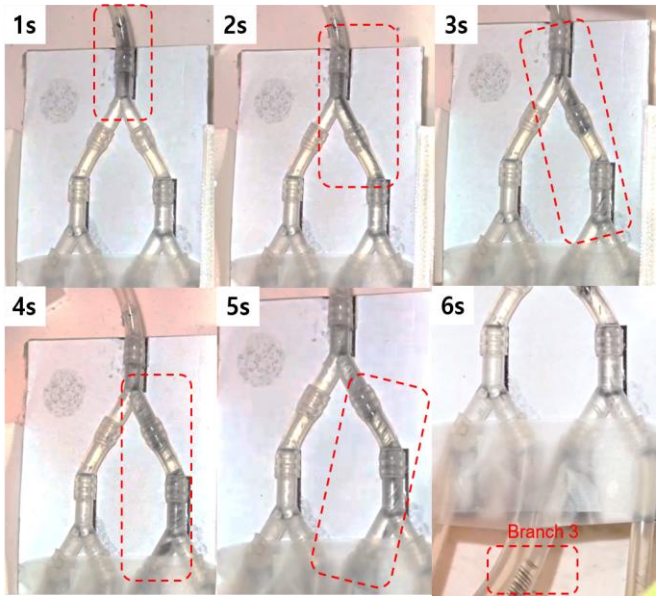

Fig. 11 The guidance process over time is illustrated, where the magnetic nanoparticle chains (black) progressively align in the same direction. As highlighted in the red dotted box, the chains exhibit consistent orientation and are directed toward Branch 3.

Fig. 11 presents time-lapse images of particle trajectories, demonstrating that MNP chains were successfully directed toward the target branch using the proposed feedforward guidance scheme. The evolutionary automatic guidance scheme achieved an average success rate of 71.59% for particles reaching Branch 3, compared to 27.92% in the absence of control (Fig. 12). In the control-free experiments, a permanent magnet was positioned at Branch 3 to mitigate particle drift, which may have slightly increased the baseline collection; nonetheless, the results clearly indicate that the proposed framework significantly enhances nanoparticle targeting efficiency, achieving effective guidance even under relatively high flow velocities.

The results further demonstrate that the guidance framework maintains robust performance across a range of initial chain positions and velocities, confirming its resilience to flow-induced perturbations. The uniformity of the magnetic force field, validated through droplet experiments, contributed directly to the reproducibility of particle trajectories, underscoring the importance of the optimized Halbach array in providing consistent actuation forces throughout the workspace.

It should be noted that the current experiments were performed in a simplified four-channel vascular model, which does not fully replicate the structural complexity of physiological vasculature. Experimental constraints, including fabrication and measurement limitations, prevented testing in more anatomically realistic geometries. Moreover, the maximum flow velocity and viscosity evaluated was limited by the strength of the permanent magnets used; stronger magnets in future implementations could potentially enable guidance under higher flow conditions, extending the practical applicability of the proposed scheme. In future work, incorporating three-dimensional rotational control of the magnetic system could allow chain orientations to be adjusted with greater degrees of freedom, enabling more precise guidance even in complex vascular environments.

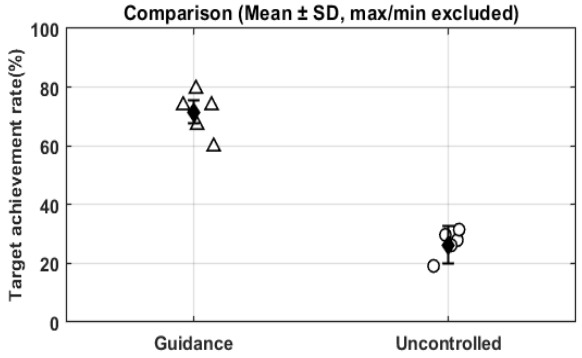

Fig. 12 Target achievement rate result. Data points represent individual values, while black diamonds indicate mean ± standard deviation calculated after excluding the maximum and minimum values.

IV. Conclusion

In this study, we introduced and validated an evolutionary automatic guidance scheme for magnetic nanoparticles (MNPs) in high-flow vascular environments, integrating optimized hardware design with simulation-based feedforward control. A hybrid dipole–quadrupole Halbach array was developed to produce a nearly uniform magnetic force field across a 70mm workspace, ensuring consistent magnetic forces regardless of the particles' initial positions.

By modeling MNPs as rigid chains, we established a physics-based simulator that captures magnetic, hydrodynamic, and wall interaction forces, enabling realistic prediction of particle dynamics. Feedforward control sequences were generated using the CMA-ES, providing globally optimized commands robust to variations in chain length and injection positions, effectively eliminating the need for real-time feedback. Experimental validation in a four-channel vascular model demonstrated the system's effectiveness: approximately 71.59% of nanoparticles successfully reached the target branch under control, a significant improvement over the 27.92% achieved without guidance.

Although currently limited to simplified models, these results confirm the feasibility of reliable MNP navigation under physiologically relevant high-flow conditions. With further advancements in 3D control strategies and stronger magnetic actuation, this guidance scheme can be expanded to anatomically realistic vascular networks. As a primary application, this strategy could facilitate targeted drug delivery through the common carotid artery, enhancing the potential for nanoparticles to cross the blood-brain barrier (BBB) for minimally invasive brain therapies.

Acknowledgment

This work was supported in part by the National Research Foundation of Korea (NRF) grant, funded by the Government of Korea (MSIT): RS-2025-00554248 and supported by AI-based GIST Research Scientist Project grant funded by the GIST: 2019-0-01842.

References

[1] M. Sitti, H. Ceylan, W. Hu, J. Giltinan, M. Turan, S. Yim, and E. Diller, "Biomedical applications of untethered milli/microrobots," Proc. IEEE, vol. 103, no. 2, pp. 205–224, 2015.

[2] B. J. Nelson, I. K. Kaliakatsos, and J. J. Abbott, "Microrobots for minimally invasive medicine," Annu. Rev. Biomed. Eng., vol. 12, pp. 55–85, 2010.

[3] X. Z. Chen, B. Jang, D. Ahmed, C. Hu, C. De Marco, M. Hoop, F. Mushtaq, B. J. Nelson, and S. Pané, "Small-scale machines driven by external power sources," Adv. Mater., vol. 30, no. 15, p. 1705061, 2018.

[4] H. Zhou, C. C. Mayorga-Martinez, S. Pané, L. Zhang, and M. Pumera, "Magnetically driven micro and nanorobots," Chem. Rev., vol. 121, no. 8, pp. 4999–5041, 2021.

[5] I. S. Khalil et al., "Positioning of drug carriers using permanent magnet-based robotic system in three-dimensional space," in 2017 IEEE Int. Conf. Adv. Intell. Mechatronics (AIM), Munich, Germany, 2017, pp. 1117-1122.

[6] L. B. Thomsen, M. S. Thomsen, and T. Moos, "Targeted drug delivery to the brain using magnetic nanoparticles," Ther. Deliv., vol. 6, no. 10, pp. 1145–1155, 2015.

[7] M. K. Manshadi, M. Saadat, M. Mohammadi, M. Shamsi, M. Dejam, R. Kamali, and A. Sanati-Nezhad, "Delivery of magnetic micro/nanoparticles and magnetic-based drug/cargo into arterial flow for targeted therapy," Drug Deliv., vol. 25, no. 1, pp. 1963–1973, 2018.

[8] O. Felfoul, A. T. Becker, G. Fagogenis, and P. E. Dupont, "Simultaneous steering and imaging of magnetic particles using MRI toward delivery of therapeutics," Scientific Reports, vol. 6, no. 1, p. 33567, 2016

[9] L. Wang, C. Gan, H. Sun, and L. Feng, "Magnetic nanoparticle swarm with upstream motility and peritumor blood vessel crossing ability," Nanoscale, vol. 15, no. 34, pp. 14227–14237, 2023.

[10] J. Jiang, L. Yang, and L. Zhang, "Closed-loop control of a Helmholtz coil system for accurate actuation of magnetic microrobot swarms," IEEE Robotics and Automation Letters, vol. 6, no. 2, pp. 827–834, 2021.

[11] H. C. Öttinger, Stochastic Processes in Polymeric Fluids: Tools and Examples for Developing Simulation Algorithms. Berlin, Germany: Springer, 2012.

[12] M. P. Bui, T. A. Le, and J. Yoon, "A magnetic particle imaging-based navigation platform for magnetic nanoparticles using interactive manipulation of a virtual field free point to ensure targeted drug delivery," IEEE Trans. Ind. Electron., vol. 68, no. 12, pp. 12493–12503, Dec. 2020.

[13] O. Baun and P. Blümler, "Permanent magnet system to guide superparamagnetic particles," J. Magn. Magn. Mater., vol. 439, pp. 294–304, 2017.

[14] P. Blümler and H. Soltner, "Practical concepts for design, construction and application of Halbach magnets in magnetic resonance," Appl. Magn. Reson., vol. 54, no. 11, pp. 1701–1739, 2023.

[15] M. Park, U. Bozuyuk, E. Yildiz, H. Min, J. Yoon, and M. Sitti, "3D locomotion of surface-rolling microrobots: A trade-off between hydrodynamic wall and gravitational effects," Adv. Intell. Syst., p. 2500381, 2025.

[16] M. Park, S. Oh, T. A. Le, and J. Yoon, "Aggregation volume estimator–based offline programming guidance of magnetic nanoparticles in the realistic rat-brain vasculature model," Adv. Intell. Syst., vol. 5, no. 9, p. 2300128, 2023.

[17] M. Park, T. A. Le, and J. Yoon, "Offline programming guidance for swarm steering of micro-/nano magnetic particles in a dynamic multichannel vascular model," IEEE Robot. Autom. Lett., vol. 7, no. 2, pp. 3977–3984, 2022.

[18] S. A. Abbasi, A. Ahmed, S. Noh, N. L. Gharamaleki, S. Kim, A. M. B. Chowdhury, et al., "Autonomous 3D positional control of a magnetic microrobot using reinforcement learning," Nat. Mach. Intell., vol. 6, no. 1, pp. 92–105, Jan. 2024.

[19] X. Du, M. Zhang, J. Yu, L. Yang, P. W. Y. Chiu, and L. Zhang, "Design and real-time optimization for a magnetic actuation system with enhanced flexibility," IEEE/ASME Trans. Mechatronics, vol. 26, no. 3, pp. 1524–1535, Jun. 2020.